Precision estimation of local offsets between pairs of SAR SLCs and detected SAR images

Charles Werner, Urs Wegmüller, Tazio Strozzi, and Andreas Wiesmann
Gamma Remote Sensing, Worbstrasse 225, CH-3073 Gümligen, Switzerland
Tel: +41 31 9517005, Fax: +41 31 9517008
Contact : Charles Werner, e-mail: cw@gamma-rs.ch

Abstract — Measurement of the offsets between SAR images is required for SAR applications including multi-temporal studies, change detection, radargrammetry (stereo), interferometry, and surface deformation. Offsets between SAR images are measured in slant range and azimuth (along-track) directions. Applications requiring offset information can be classed into those that require only a global offset function and those, such as radar stereo and deformation mapping that require localized individual measurements. This paper describes our investigation to improve the accuracy of single measurements. The offset estimation algorithm is described. Over-sampling of the Single-Look Complex (SLC) data prior to estimating the offsets improves accuracy substantially. Estimates of the offset errors including offset dependent bias are evaluated using data from ERS.

Keywords: SAR interferometry, glacier velocity, radargrammetry, earthquake motion, offset measurement.

I. INTRODUCTION

Analysis of remote sensing data requires co-registration of image data for multi-temporal studies, mapping topography, and comparison of data acquired using different sensors. There are numerous SAR applications that require coregistration and resampling including multi-temporal studies and change detection [1], interferometry [2]-[4], terrain geocoding [5], radargrammetry (stereo) [6]-[8], and mapping of surface deformation [9]-[13]. Particularly radar stereo and mapping of surface deformation have recently gained in importance. Surface deformations due to glacier motion and earthquakes have been successfully mapped using SAR image offsets. Applications where offsets are used to determine surface deformation or local topography require estimation algorithms that are unbiased, accurate, and robust. This has been our motivation to improve the accuracy of single offset measurements while maintaining efficiency. In the following sections we describe an improved offset algorithm and the results of tests for bias and accuracy.

The offset between a pair of SAR images is a function of the SAR image processing parameters, orbital tracks, scene topography, and surface displacement that occurred during the interval between data acquisitions. In the absence of both deformation, and stereo offsets due to substantial topography and large orbit separation, the range and azimuth offsets vary smoothly over the image [2]. Applications such as interferometry, change detection, and SAR geocoding use offset measurements to derive a polynomial model to evaluate the offset for every point in the scene. Offsets measured on a regular grid are used to estimate the parameters of a bi-linear model of the offsets used to resample one of the images. Measurements that do not meet a predetermined correlation threshold are discarded. The offset model is then used to accurately resample the second image to match the reference scene. Interferogram formation requires that images be coregistered with an accuracy of better than 1/8 pixel to avoid significant loss of phase coherence [3][4].

II. OFFSET ALGORITHM DESCRIPTION

Offsets are measured using patches that are M_1 x M_2 (range x azimuth) pixels at a set of positions in the scene. The locations are uniformly distributed over the image frame when offset data are used for determining a polynomial offset function, while for deformation mapping; a specific region can be selected for dense sampling. In both cases, an initial constant offset in range and azimuth is determined for the entire scene using orbit information or by estimating the offset for a large image patch. The residual offset after this initial step should not be larger than a small fraction of the patch size that will be used for measuring the offset field. Typical values for M_1 and M_2 are in the range of 16 to 256 depending on the noise level and specific application. Data covering the patch is extracted from each SLC and any range or azimuth phase gradients are estimated and removed. Next, the patch SLC data are over-sampled by a factor of 2 or 4 using FFT interpolation [14].

Note that the power spectrum of the intensity image $I_1 = S_1 S_1^*$ has twice the bandwidth of the SLC before detection. Hence over-sampling of the SLC by a factor of 2, or more, prior to detection eliminates aliasing due to the increased bandwidth as a source of noise. Over-sampling also has the added benefit of improving the sampling of the desired correlation function obtained from the patch data. The location of the maximum of the 2D correlation function yields the desired range and azimuth offsets. The correlation function $C(n_1, n_2)$ is defined as:

$$R(n_1, n_2) = \sum_{0}^{M_1} \sum_{0}^{M_2} I_1(m_1 + n_1, m_2 + n_2) I_2^*(m_1, m_2), \quad (1)$$

where I_1 and I_2 are the detected over-sampled SLC data $S_1 S_1^*$ and $S_2 S_2^*$ respectively. The correlation is most efficiently implemented using a 2D FFT, since it is known that:

$$R(n_1, n_2) = FFT^{-1}\left[\tilde{I}_1(m_1, m_2)\tilde{I}_2^*(m_1, m_2)\right] \quad (2)$$

The function $R(n_1,n_2)$ samples the correlation function at 0.5 or 0.25 pixels when the over-sampling factor (OSF) is 2 or 4. To obtain an accurate estimate of the correlation peak, the

correlation function values over a 3x3 region are fit using a bi-quadratic polynomial surface. The SNR of the offset measurement is obtained by taking the ratio of the peak value divided by the average correlation level outside the 3 x 3 peak region.

Alternately, it is possible to cross-correlate the SLC patches without detection and preserve the SLC phase information. In this case the complex correlation function is given by:

$$R(n_1, n_2) = \sum_{0}^{M_1} \sum_{0}^{M_2} S_1(m_1 + n_1, m_2 + n_2) S_2^*(m_1, m_2) e^{-j(am_1 + bm_2)} \quad (3)$$

This method depends on being able to remove the interferometric phase by multiplying by a complex exponential function. Otherwise, the correlation magnitude will be substantially reduced. A 2D FFT of the patch interferogram is used to estimate the linear and azimuth phase slopes a and b for each value of the offset indices n_1 and n_2. This approach may give improved results for small patches in areas with low contrast.

III. OFFSET ESTIMATION BIAS AND ACCURACY

The offset measurements may have offset dependent errors. This bias error arises due to under-sampling of the correlation function $R(n_1,n_2)$. A simulation was performed to estimate this type of error. A section of an ERS SLC was resampled using a SINC interpolator to apply a linear stretch of -1 to +1 pixel in both range and azimuth. Then the offsets at 128 points were measured across the swath between the resampled and original SLCs. Figs. 1 and 2 show regressions of the range offset measurements for over-sampling factors (OSF) of 1 and 2. The standard deviations of a fit of the measured range offsets relative the known offset function are given in Table 1.

The deviations from the true regression line follow a sinusoidal pattern in the case OSF = 1 as the offset changes by 1 pixel in range. Note that the measurements are noisier around offset values of -.5 and +.5 samples. In these regions the correlation values are least accurate because the peak of the correlation function lies halfway between samples. The s of the offset measurements drops substantially for OSF factors of 2 or more.

In a further test for offset bias, single-look multi-look intensity data were used as the starting point rather than SLC data. The test image was calculated from the stretched SLC from the first test. In the OSF = 2 case, the s for the range offset measurements increased to .0347 pixels.

A further test was performed to evaluate offset errors between different SLCs. The test data were from a tandem ERS interferometric pair with small baseline acquired over a desert region. Offsets were measured using M_1=32, M_2=32 for 1024 patches distributed over the scene. Of these, 974 had SNR values greater that the minimum SNR threshold of 6.5. A summary of the offset fit residuals is shown in Table 2. A typical set of offset measurements across the swath is shown in Fig 3. Range and azimuth offset accuracies better than 1/30 (1s) pixel were obtained.

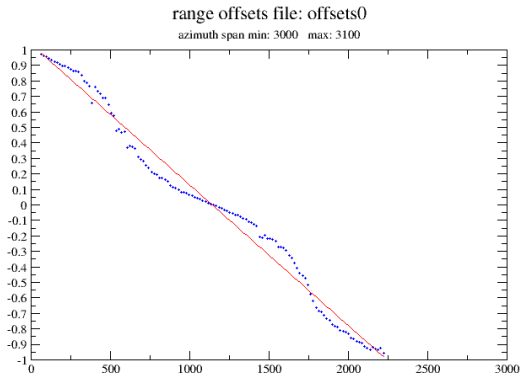

Fig. 1. Offset estimation, no SLC over-sampling (OSF = 1) N=128, M_1=64, M_2=64

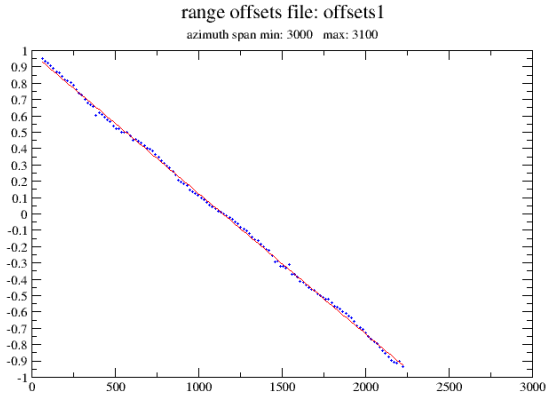

Fig. 2. Offset estimation with SLC over-sampling factor 2 (OSF = 2) N=128 M_1=64, M_2=64

SLC OSF	s Range Offset
1	0.0777
2	0.0156
4	0.0105

Table 1. Range offset estimation bias for interferometric ERS SLC data, SNR threshold = 6.5, M_1=64, M_2=64

SLC OSF	s Range Offset	s Azimuth Offset
2	.0262	.0330
4	.0202	.0271

Table 2. Range and azimuth offset residuals as a function of OSF for an interferometric image pair, M_1=32, M_2=32, SNR > 6.5

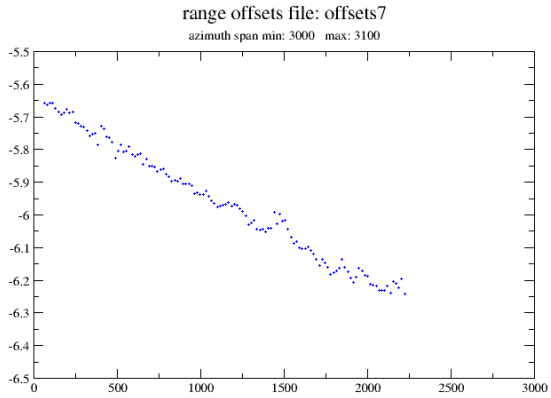

Fig.3. Range offsets measured across track for an ERS SLC pair over desert (N=128, M_1=32, M_2=32, OSF = 4)

Range and azimuth offset maps of a region of a glacier in the Antarctic were created to demonstrate the ability of the offset estimator to robustly map regions with large surface deformation. The range and azimuth offset data are displayed with a periodic color scales, 3 pixels per cycle (Fig. 4 and 5). Data were acquired on 24-Sep-1997 and 18-Oct-1997 using Radarsat-1 operating in ST2 mode. Offsets were measured over an area that is 115.8 km in range x 31 km in azimuth with a pixel spacing of 8.117 m (range) and 5.333 m (azimuth). Offset measurements are spaced at 160 m in both North and East directions. The offset maps have been geocoded such that North is up. In this rapidly moving area of the glacier, the motion exceeds what can be measured interferometrically.

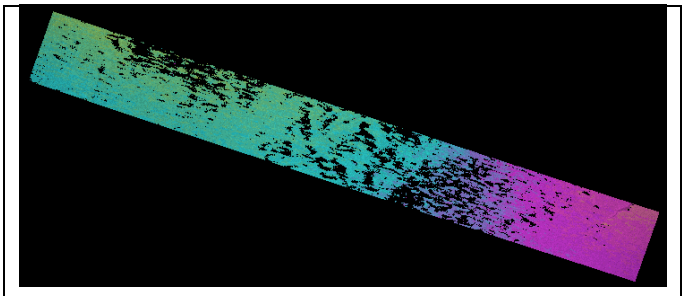

Fig 4. Slant-range offset map for a segment of an Antarctic glacier. 1 color cycle = 3 slant range pixels (24.35 m)

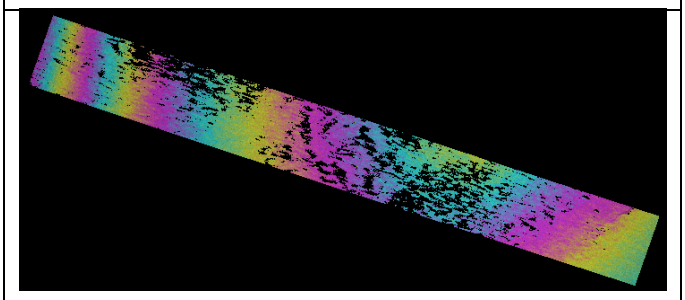

Fig 5. Azimuth offset map for a segment of an Antarctic glacier. 1 color cycle = 3 azimuth pixels (16 m)

IV. Conclusions

The algorithm presented in this paper is able to measure azimuth and range offsets for ERS data with accuracy better than 1/30 pixel in range and azimuth. This is equivalent to offsets of 13 cm in azimuth and 26 cm in slant range. Bias errors and noise due to aliasing can be reduced by over-sampling the SLC image data prior to cross correlation. Particularly applications in deformation mapping and SAR stereo applications that require individual localized measurements can use this algorithm for production of data products.

V. Acknowledgements

Thanks to Neal Young of the University of Tasmania Antarctic Climate and Ecosystems Cooperative Research Centre for helpful discussions and making the data available for the Antarctic glacier offset map.

ERS SAR data ©ESA, Radarsat data ©RSI

VIII. References

[1] Wegmüller U., C. Werner, and R. Cordey, "Flashing fields! A preliminary investigation", Proc. ENVISAT Symposium 2004, Salzburg, Austria, 6-10 Sep. 2004.

[2] P.Rosen et al., "Synthetic Aperture Radar Interferometry," *Proc. IEEE* vol. 88, no. 3, pp. 333- 382, 2000.

[3] Hanssen, R, "Radar Interferometry, Data Interpretation and Error Analysis," Kluwer Academic Publishers, Dordrecht, pp. 45-47, 2001.

[4] Werner C., U. Wegmüller, T. Strozzi, and A. Wiesmann, "*Gamma* SAR and Interferometric Processing Software", Proceedings of ERS-ENVISAT Symposium, Gothenburg, Sweden, 16-20 Oct. 2000.

[5] U. Wegmüller, "Automated Terrain Corrected SAR Geocoding," Proceedings IGARSS'99, Hamburg, 28 June - 2 July 1999 (CC03_02).

[6] Toutin, Th, L. Gray, "State-of-the-art of elevation extraction from satellite SAR data," ISPRS J. of Photogrammetry & Rem. Sens., vol. 55, pp.13–33, 2000.

[7] Wegmüller U., C. Werner, A. Wiesmann, and T. Strozzi, "Radargrammetry and space triangulation for DEM generation and image ortho-rectification", Proc. IGARSS 2003, Toulouse, France, 21-25 July 2003.

[8] M. Gelautz et. al, "A Comparative Study of Radar Stereo and Interferometry for DEM Generation," Proceedings of ESA FRINGE 2003 Workshop, 1-5 Dec 2003, ESA SP-550, 2004.

[9] Strozzi et. al, "Glacier Motion Estimation Using SAR Offset-Tracking Procedures," IEEE Trans. Geosci, Remote Sensing, vol. 40, no. 11, pp 2385-2391, Nov, 2002.

[10] Joughin, I. "Ice sheet velocity mapping: A combined interferometricand speckle tracking approach, Ann. Glaciol., vol. 34, pp.195–201, 2002.

[11] Gray, A. L., et al. "InSAR Results from the RADARSAT Antarctic Mapping Mission Data: Estimation of Glacier Motion using a Simple Registration Procedure," Proceedings of IEEE IGARSS 98 Conference, IEEE, pp. 1638-1640, 1998

[12] Michel, R.., J. Avouac, and J. Taboury, "Measuring near field coseismic displacements from SAR images: Application to the Landers Earthquake," Geophys. Res. Lett., vol. 26, pp. 3017– 3020, 1999.

[13] Fialko, Y., M, Simons, and D. Agnew, "The complete (3-D) surface displacement field in theepicentral area of the 1999 Mw7.1 Hector Mine earthquake, California, from space geodetic observations," Geophys. Res. Lett., vol. 28, pp. 3063-3066, 2001.

[14] Rabiner, L. and B. Gold, "Theory and Application of Digital Signal Processing," Prentice Hall, Englewood Cliffs, New, Jersey, pp 50-59, 1975.